

---

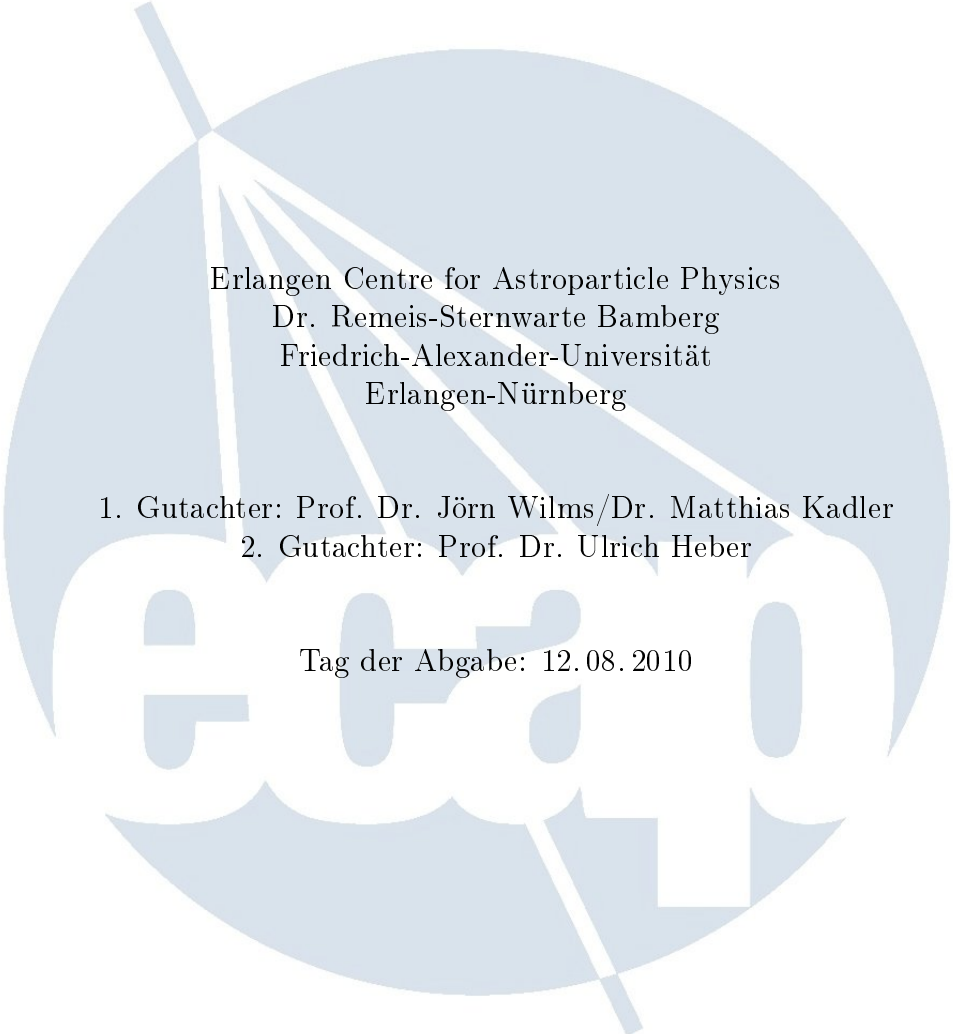
# Swift Observations of TANAMI Counterparts

---

---

Bachelorarbeit

vorgelegt von  
Felicia Krauß



Erlangen Centre for Astroparticle Physics  
Dr. Reimis-Sternwarte Bamberg  
Friedrich-Alexander-Universität  
Erlangen-Nürnberg

1. Gutachter: Prof. Dr. Jörn Wilms/Dr. Matthias Kadler
2. Gutachter: Prof. Dr. Ulrich Heber

Tag der Abgabe: 12.08.2010

# Contents

<b>1</b>	<b>Introduction</b>	<b>1</b>
1.1	AGN . . . . .	1
1.1.1	History . . . . .	1
1.1.2	Unified Model . . . . .	1
1.1.3	Accretion . . . . .	4
1.2	Blazars and Jets . . . . .	4
1.3	The TANAMI Project . . . . .	6
<b>2</b>	<b>Datareduction</b>	<b>8</b>
2.1	SWIFT . . . . .	8
2.2	XRT . . . . .	9
2.3	Data reduction . . . . .	10
<b>3</b>	<b>Observations and Analysis</b>	<b>12</b>
3.1	Overview/ Introduction . . . . .	12
3.2	Bright sources . . . . .	14
3.3	Weak sources . . . . .	28
3.4	Analysis . . . . .	29
3.4.1	Photon indices . . . . .	29
3.4.2	Absorption . . . . .	30
<b>4</b>	<b>Summary and Outlook</b>	<b>30</b>
<b>5</b>	<b>Appendix</b>	<b>31</b>
5.0.3	Added Spectra . . . . .	31

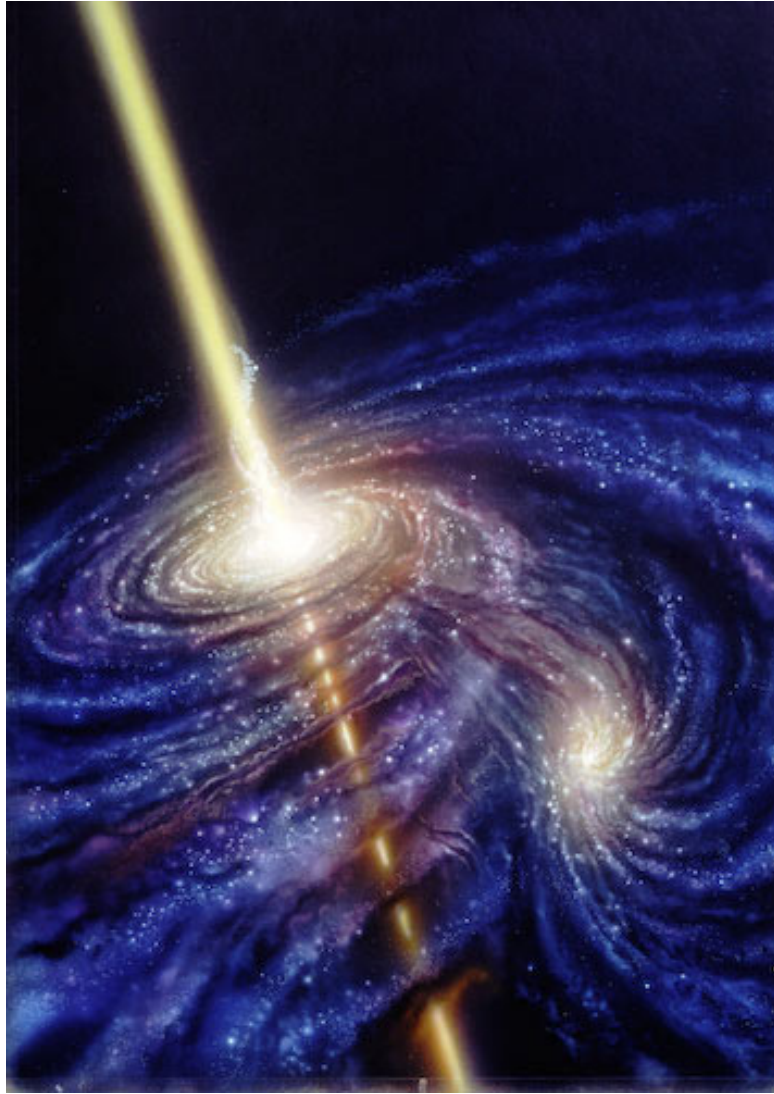


Figure 1: An artists' conception of an Active Galactic Nuclei

(<http://www.cosmographica.com>)

## Abstract

In this bachelor thesis a sample of Active Galactic Nuclei data is analyzed. The data are from the NASA satellite Swift, or to be more precise, from the XRT instrument which collects X-Ray information. The sources are part of the TANAMI sample, a VLBI program which monitors AGN on the Southern Hemisphere at radio frequencies. 10 of 23 sources could be modeled in detail. In the following thesis the results of these 23 sources are discussed in detail. The fit parameters are furthermore discussed. Results include a low absorption as well as a high number of LBLs that have been detected.

# Chapter 1

## Introduction

### 1.1 AGN

#### 1.1.1 History

AGN were first remarked on in 1908 by Edward A. Fath who found emission lines in NGC 1068 to be similar to a planetary nebula. (Fath, 1909) A decade later Heber D. Curtis wrote „M87 exhibits a curious straight ray...apparently connected with the nucleus by a thin line of matter“ (Curtis, 1918).

This was the first time an optical jet of a galaxy was observed. Many years later multi-wavelength campaigns found those jets to be visible in many wavebands. In 1943 Carl Seyfert classified spiral galaxies with optical emission lines (Seyfert, 1943). Today these are called Seyfert galaxies. In 1954 Walter Baade and Rudolph Minkowski discovered the optical counterparts to the radio sources Cygnus A, Virgo A and Puppis (Baade & Minkowski, 1954). As of today many aspects of active galactic nuclei still remain a mystery.

#### 1.1.2 Unified Model

Active Galactic Nuclei can be characterized by their optical spectra into 2 Types. Type 1 AGN have broad and narrow emission lines superposed on a continuum. Broad emission lines come from allowed transition with widths of up to  $10^4 \text{ km s}^{-1}$ . This suggest the presence of a dense medium with high velocities. ( $n \sim 10^9 \text{ cm}^{-3}$ ) The narrow emission lines are due to forbidden transitions with small widths. Forbidden transitions always points to a low density medium ( $n \sim 10^3 \text{ cm}^{-3} - 10^6 \text{ cm}^{-3}$ ). An example of an optical spectrum of a Type 1 AGN is shown in Figure 1.1 (Peterson, 2009).

Type 2 AGN exhibit narrow lines superposed on a weak continuum but no broad lines. This suggest a low density medium along the line of sight. This is shown in figure 1.2 (Sanderson, 2007).

The Unified model tries to explain both spectra with one type of galaxy. It states, that whether a Type 1 or 2 is observed depends on the angle of the observer to the axis of symmetry. However,

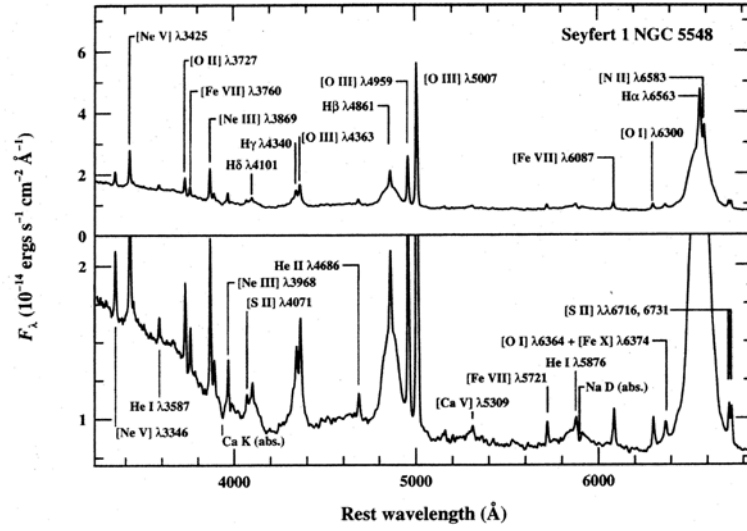


Figure 1.1: Optical Spectrum of NGC 5548

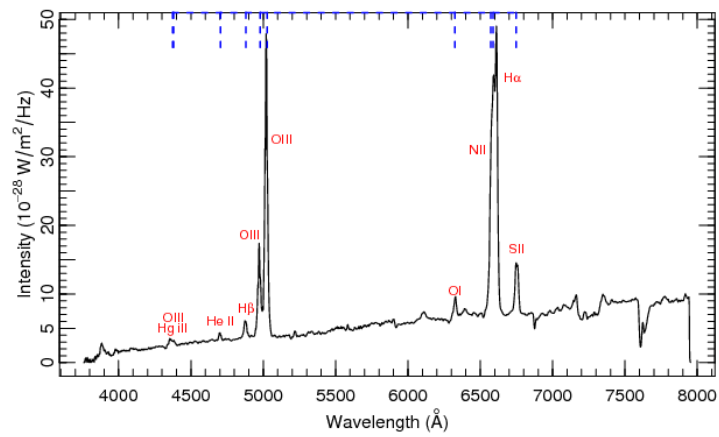


Figure 1.2: Optical Spectrum of M77

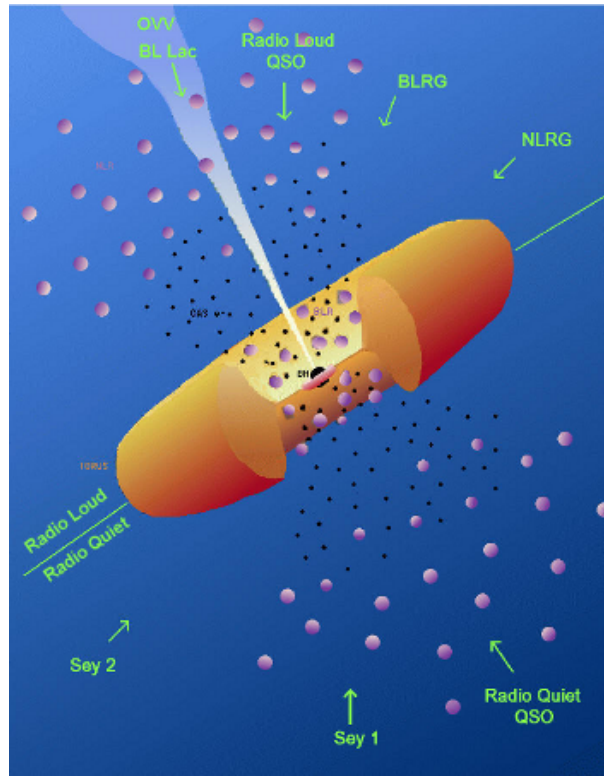


Figure 1.3: Active Galactic Nuclei: Unified Model

there are more than just two types. AGNs in general are characterised by their high luminosity as well as a nonthermal spectrum. The AGN Continua are powerlaws with

$$F_\nu = \nu^{-\alpha} \quad (1.1)$$

where the photon index is  $\Gamma = \alpha + 1$ . If  $\nu F_\nu$  is constant, same amounts of energy are emitted per frequency decade. The emission is nonthermal.

The unified model shows that Seyfert Galaxies, QSO's, Quasars and Blazars are all the same type of galaxy. The theory of the unified model states that the angle of the observer to the axis of symmetry decides on what we observe. As it can be seen in figure 1.3 (Urry & Padovani, 1995), AGN Type 1 allow for a direct view onto the Black Hole and the Accretion Disk, whereas AGN Type 2's view of the center is obscured by a dust torus. This explains the emission lines that are seen in the optical spectra in Figure 1.1 and 1.2. In the type 1 spectra the broad emission lines as well as the narrow lines are visible. In the type 2 spectra the Broad Line Region, emitting the broad lines, is obscured by the torus. Thus only narrow lines are visible. The difference between a Seyfert Galaxy and a QSO is only the luminosity. QSO's are more luminous than Seyfert Type 1 and 2.

Radio Galaxies are AGN that are bright in the Radio waveband. (But: all AGN emit in the Radio) Radio-loud AGN usually have Jets.

The Broad Line Radio Galaxy (BLRG), Narrow Line Radio Galaxy (NLRG), Quasar Type 1 and 2 are the radio-loud equivalents to the Seyfert 1, 2 and QSO Type 1 and 2 respectively.

### 1.1.3 Accretion

The general accepted theory states that the high luminosity in AGN is fuelled by supermassive black holes in their center. The accretion process has an upper limit, the Eddington limit which is derived by stating that the gravitational force in an accretion disk has to dominate the radiation pressure, else there would be no material falling into the black hole.

$$L < L_{\text{Edd}} = \frac{4\pi GMm_p c}{\sigma_T} = 1.3 \cdot 10^{38} \text{ erg s}^{-1} \cdot \frac{M}{M_{\odot}}$$

with the luminosity  $L$ , the gravitational constant  $G$ , the mass of the black hole  $M$ , the mass of a proton  $m_p$  and the Thomson cross-section  $\sigma_T$ . Accretion can be characterized by its efficiency.

$$L = \eta \cdot \dot{M} c^2$$

with the mass accretion rate  $\dot{M}$ . From those equation follows the maximum mass accretion rate of

$$\dot{M}_{\text{max}} = \frac{L_{\text{Edd}}}{\eta \cdot c^2}$$

If energy would be produced through fusion the efficiency can be calculated.

$$\Delta E_{\text{nuc}} = \frac{(m_{\text{He}} - 4 \cdot m_p) \cdot c^2}{4} = \eta \cdot m_p \cdot c^2$$

This results in an efficiency of 0.007 of the rest mass of the proton. The accretion power equals  $\approx 6 \cdot 10^{11} \text{ J g}^{-1}$ .

However the efficiency of the accretion is given through:

$$\Delta E_{\text{acc}} = \frac{GMm}{R_S}$$

with  $R_S = 2GM \cdot c^{-2}$  being the Schwarzschild radius. This results in an efficiency of 0.1 of the rest mass of the proton. The accretion power is given through  $\approx 10^{13} \text{ J g}^{-1}$ . This shows very clearly that accreting matter is a very efficient energy source, as an accretion rate of  $1 \dots 2 M_{\odot} \text{ yr}^{-1}$  is sufficient to power a black hole in the center of an AGN.

## 1.2 Blazars and Jets

As mentioned in the Unified model Chapter, Jets seen at a very small angle to the line of sight are called Blazars. The word Blazar was coined by E. Spiegel in 1978 as a combination of both words, emphasizing the „blazing“ property of AGNs. Many blazars show strong variability on scales of intra-hour/intra-day to months and years. The first Blazar that was discovered was BL Lacertae or BL Lac and thus a whole category of Blazars are classified as BL Lacs. The other category is OVV quasars (optical violent quasars). All BL Lacs are also radio sources.

There are several relativistic effects in jets. For one the apparent superluminal motion. „Blobs“ of jets seem to move faster than the speed of light, due to the angle between the observer and the direction of movement.

Ghisellini describes, that the power emitted in a jet is on the order of one magnitude higher than the power emitted by the Accretion Disk (Ghisellini, 2009). They also found out that energy of emitted electron pairs do not suffice in describing the jet. Blazar Spectra are nonthermal spectra that generally look as shown in Figure 1.2.

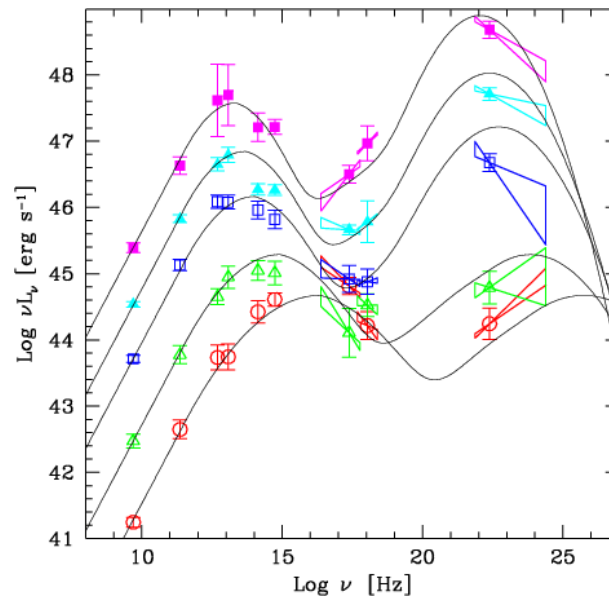


Figure 1.4: Blazar Spectra

The left hump is due to synchrotron photons in the Jet that are produced through electrons that have been accelerated. The right hump is due to Synchrotron Self - Compton (SSC) where the photons are upscattered to high energies. This scattering happens with the same electrons that produced the photons in the first place. It is generally accepted that the low energy peak is due to the synchrotron emission in the jet. The synchrotron peak is anticorrelated with the luminosity of the source. However the origin of the second peak is discussed.

For compton scattering following equation holds.

$$E_{compt} = \gamma^2 E_{primary}$$

There are two models to describe the jets, a hadronic and a leptonic model. The leptonic model suggests upscattered photons by the electrons that produced them or external electrons, e.g. from the BLR. The hadronic model suggest highly energetic proton collisions and pair production. A higher luminosity leads to a harder X-ray spectrum and a softer  $\gamma$ -ray spectrum. This means the peak frequencies are not independent. Note that the X-ray band of the spectrum is close to the valley of the two humps. This means that from the photon index of the powerlaw the slope can be determined and thus whether the observed source is a LBL or HBL. A blazar observed with a falling slope is likely to be a high peaked frequency blazar (HBL). On the other hand a low peaked frequency blazar (LBL) is observed if the flux has a rising slope.

If on the other hand the observed blazar would lie in the deep of the valley, the flux would be the lowest and thus it would be difficult to detect the source. HBL have a generally low luminosity but high peak frequencies.

### 1.3 The TANAMI Project

Tracking Active Galactic Nuclei with Austral Milliarcsecond Interferometry (TANAMI) is a collaboration of several countries to study AGNs with an emphasis on the parsec-scale structures in jets. This project is led by M. Kadler and R. Ohja. TANAMI is using the Australian/South-African Long Baseline Array (LBA+) with the antennas at Parkes (64m), ATCA ( $5 \times 22\text{m}$ ), Mopra (22m), Hobart (26m), Ceduna (30m) and the associated antennas Tidbinbilla (DSN 70m or 34m), the IVS antennas TIGO (6m) and O'Higgins (9m) and Hartebeesthoek (26m). The aim is to image and monitor jets of AGN on the Southern Hemisphere, complementary to the MOJAVE project on the Northern Hemisphere. (Kadler, 2010)

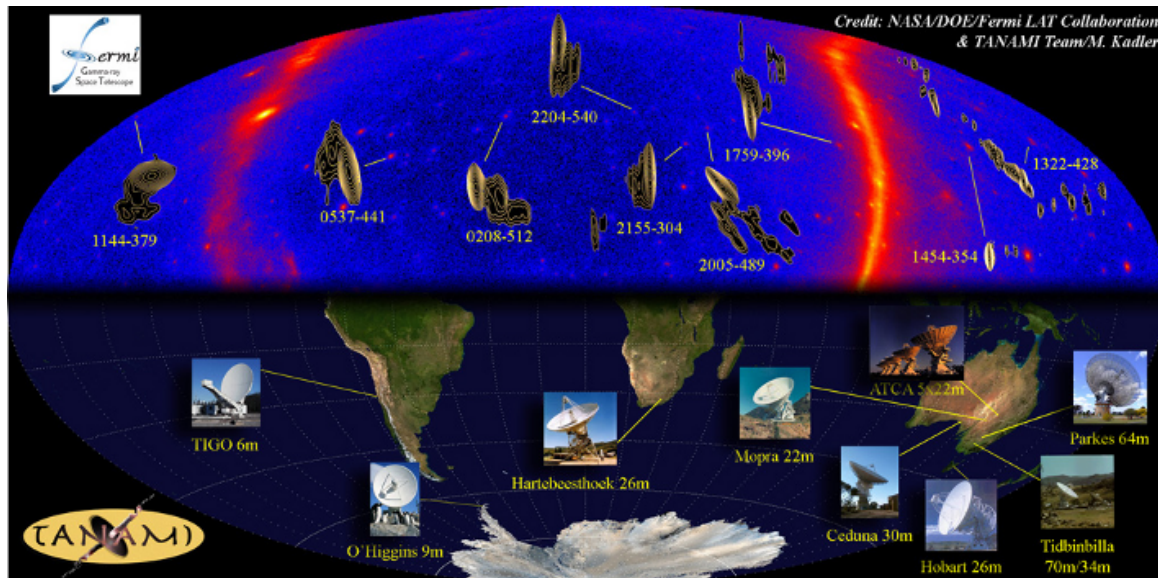


Figure 1.5: TANAMI Project

TANAMI is monitoring sources south of  $-30$  degrees at 8.4 GHz and 22 GHz. Results include samples with superluminal moving jets. TANAMI is also emphasizing the multiwavelength aspect. Observations of the Large Area Telescope (LAT) aboard the Fermi satellite in the  $\gamma$ -ray as well as X-ray, UV and optical observations by the Swift satellite (see Chapter 2) are added to the TANAMI data to create spectral energy distributions (SED). TANAMI is also monitoring newly detected sources that are flaring and have been detected with Fermi.

73 TANAMI sources have been detected by Fermi within a year, including all 10 BL LAC sources, whereas only 24 out of 32 quasars have been detected.

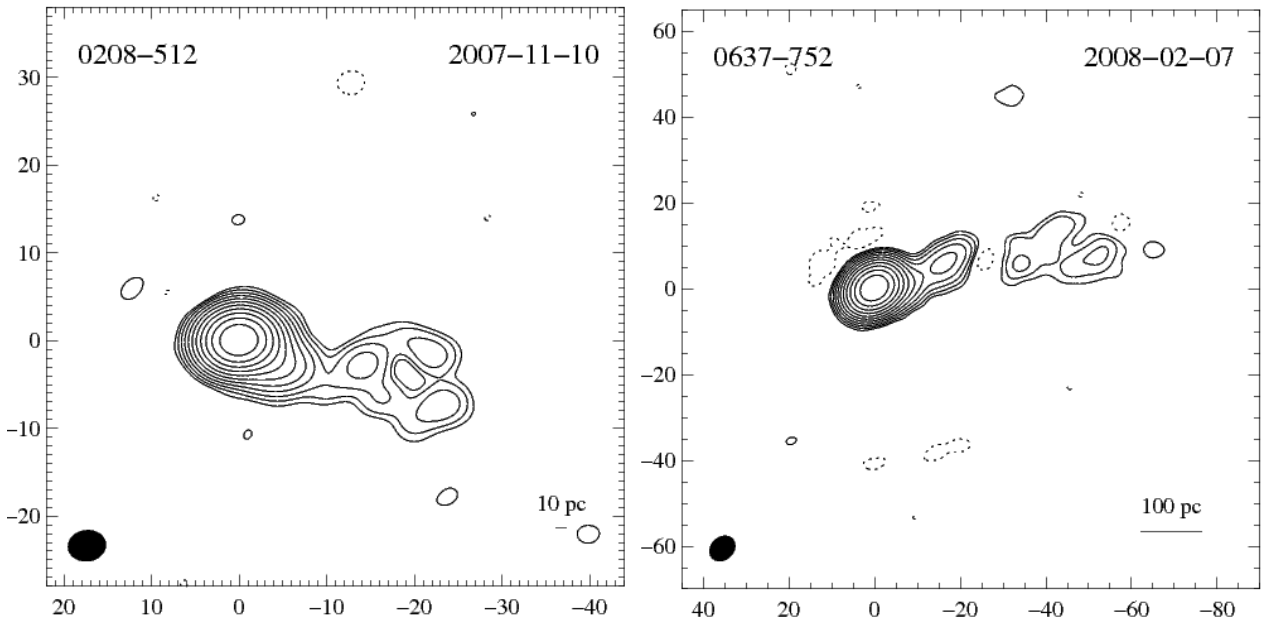


Figure 1.6: TANAMI results

Figure 1.6 (Ojha et al., 2010a) shows results from the first epoch of images at 8.4 GHz. The jets in both sources are visible on a parsec scale. These sources are later analyzed in the X-ray. The initial TANAMI sample of 43 sources has been expanded to 75 sources. 55 of these have been detected by Fermi. (Boeck et al., 2010)

## Chapter 2

# Datareduction

### 2.1 SWIFT

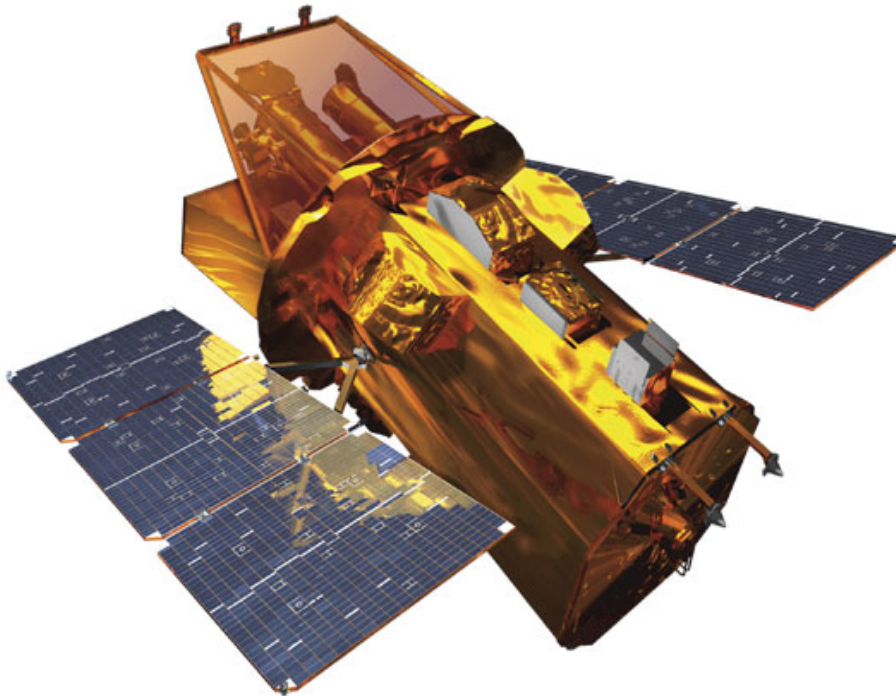


Figure 2.1: SWIFT satellite

(<http://swift.sonoma.edu/resources/multimedia/images/>)

NASA's Swift satellite was launched on 20 November 2004. It is managed by the NASA Goddard Space Flight Center and its main mission was to detect and observe Gamma – Ray Bursts in Gamma-Ray, X-Ray, optical and UV. Swift has 3 main instruments on board, the BAT (Burst Alert Telescope), the XRT (X-Ray Telescope) and the UVOT (Ultra-Violet and Optical Telescope). Swift is orbiting the earth on a low earth orbit with an orbital period of  $\approx 95$  minutes at an inclination of 20.6 degrees.

## 2.2 XRT

All observations in the next chapter used were taken with the XRT instrument. The XRT consists of a Wolter 1 Telescope, as well as an EEV CCD-22. (Holland, 2010) Most observa-

Table 2.1: Swift Properties

Property	Description
Telescope	JET - X Wolter I
Focal Length	3.5 m
effective Area	110 cm <sup>2</sup> at 1.5 keV
Detector	EEV CCD-22, 600 · 600 pixel
Operations	Imaging, Timing and photon counting
Energy Range	0.2 - 10 keV

tions were in the photon counting mode although a few were in the window-timing mode. The photon-counting mode gives full spectral and special information - a 2 dimensional image is created, although it takes more time to read out (2.5 s). This mode is used for very low fluxes. The window timing mode only gives one dimensional information but has a fast readout speed (2.2 ms). This mode is useful for low fluxes because of pileup. A pileup happens if 2 or more photons deposit charge in one pixel between two read-outs. The CCD cannot distinguish between the photons.

The following plot shows the effective area of the detector. The feature at 0.52 keV is due to an oxygen transition in the surface of the detector. At 1.84 keV is a Silicon edge of a K-shell transition. The 2.2 keV edge is due to a change in the reflectivity of the gold mirrors of the Wolter telescope.

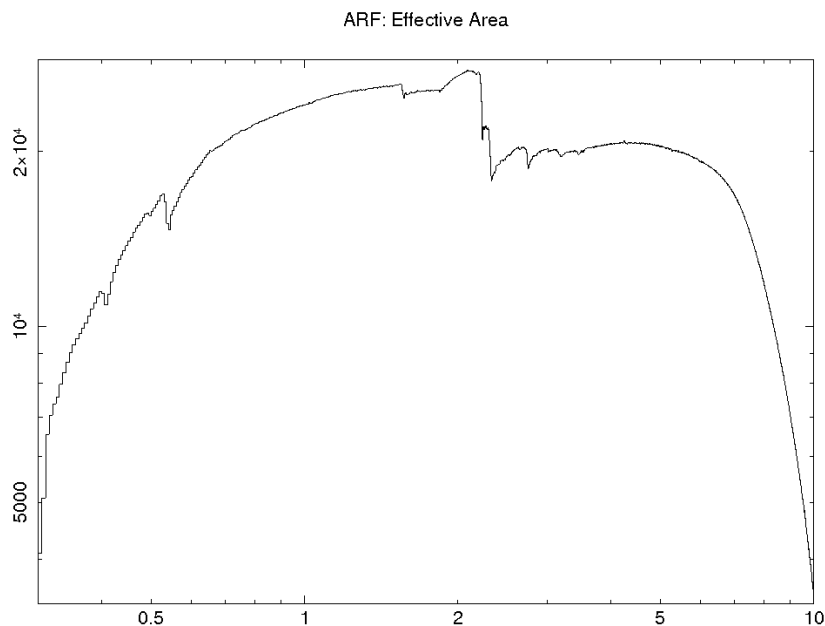


Figure 2.2: effective area

Figure 2.3 shows a plot of the response matrix at 6 (black) and 8 (red) keV.

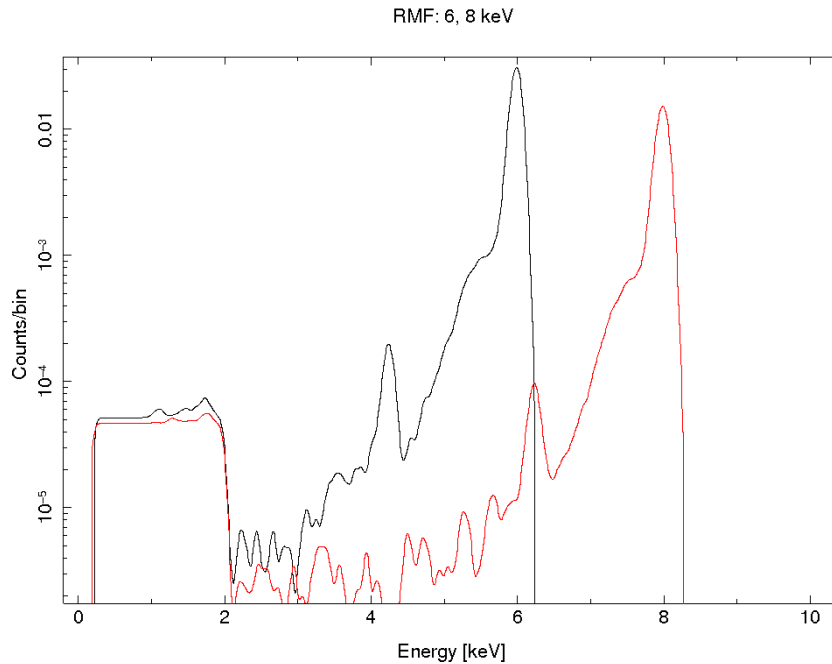


Figure 2.3: RMF at 6 and 8 keV

At both energies a Compton shoulder is visible. There is an escape peak at 2 keV minus the original photon energy. An escape peak is visible due to the escape of a fluorescence photon of the K transition in the detector material. The transition needs exactly the 2 keV and the photon is detected in the escape peak.

## 2.3 Data reduction

The data reduction was done using scripts, written mostly by Laura Barragán. These scripts correct the data for bad pixels and other errors. For background subtraction a source and a background region was defined with the help of the program ds9. At first sources were identified with the help of a script that imports source informations from Simbad (<http://simbad.u-strasbg.fr/simbad/>) into ds9, written by Jörn Wilms. After the sources had been identified regions were chosen. The source and the background region always had the same size. The source region was chosen in a way to ensure that all source counts were inside the circle. After background subtraction the data could be analyzed.

Following is an example of how the background and source region were chosen. Figure 2.4 shows PKS 0055 – 328, a weak source that was barely visible and could not be fitted. However, figure 2.5 shows PKS 0447 – 439, a bright source that could be modeled.

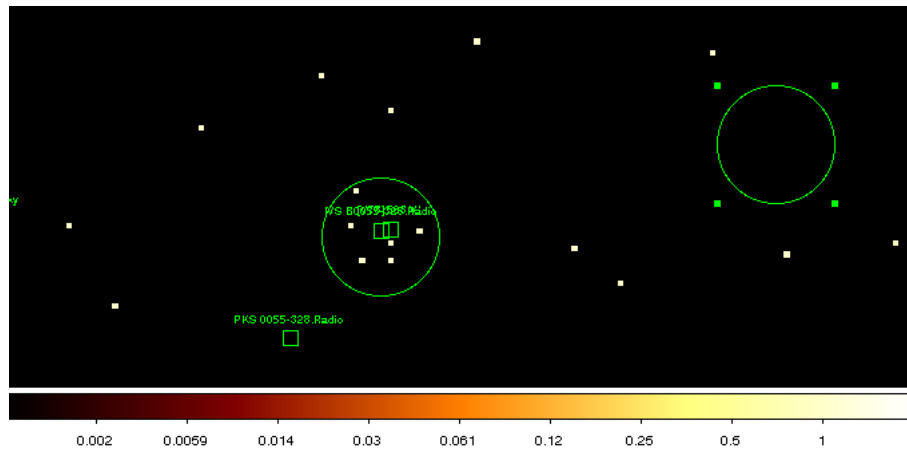


Figure 2.4: Source and background region

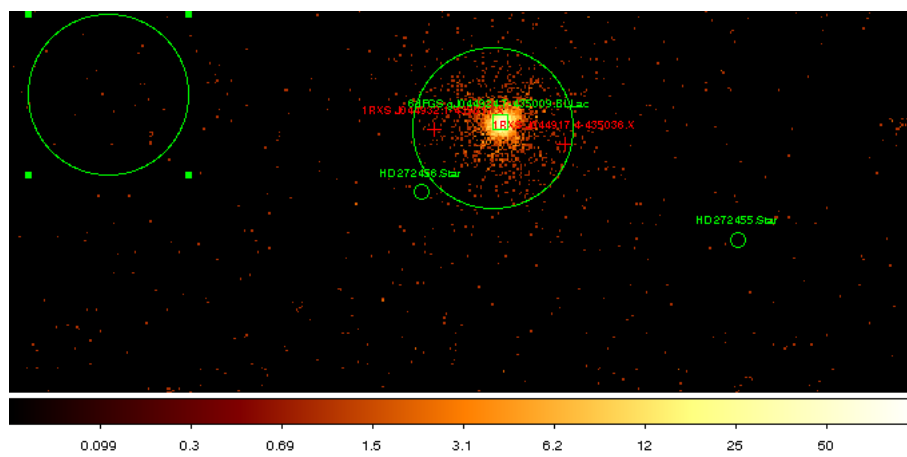


Figure 2.5: Source and background region

# Chapter 3

## Observations and Analysis

### 3.1 Overview/ Introduction

In this chapter I will explain how I analyzed the data with ISIS and what informations can be gathered about each source. A few observations had a short exposure time and were barely visible. This is why some observations could not be modeled in greater detail. Generally I fitted a powerlaw multiplied with a photon absorption.

$$N_{\text{ph}}(E) = \text{phabs} \cdot \text{powerlaw} = e^{-N_{\text{H}} \cdot \sigma_{\text{ism}}} \cdot C \cdot E^{-\Gamma}$$

with a norm  $C$ , a photon Index  $\Gamma = \alpha + 1$ , a neutral hydrogen column  $N_{\text{H}}$  and a cross-section  $\sigma_{\text{ism}}$ . I froze the photon absorption parameter  $N_{\text{H}}$  to the value of the galactic absorption to compare the results. For the values of  $N_{\text{H}}$  absorption in our Galaxy I used the information of the Leiden/Argentine/Bonn Galactic HI Survey. ([http://www.astro.uni-bonn.de/~webaiub/english/tools\\_labsurvey.php](http://www.astro.uni-bonn.de/~webaiub/english/tools_labsurvey.php))

All errorbars are given at 90% confidence. The errorbars of the average of the parameters were calculated through Gaussian error propagation. At first spectra of the observations were plotted with ISIS. Figure 3.1 shows an example of a spectrum, in this case PKS 0055 – 328, that was too weak for any grouping or fitting. Figure 3.2 shows a bright example of a spectrum, that was later grouped and fitted. All coordinates are decimal rightascension, declination (J2000).

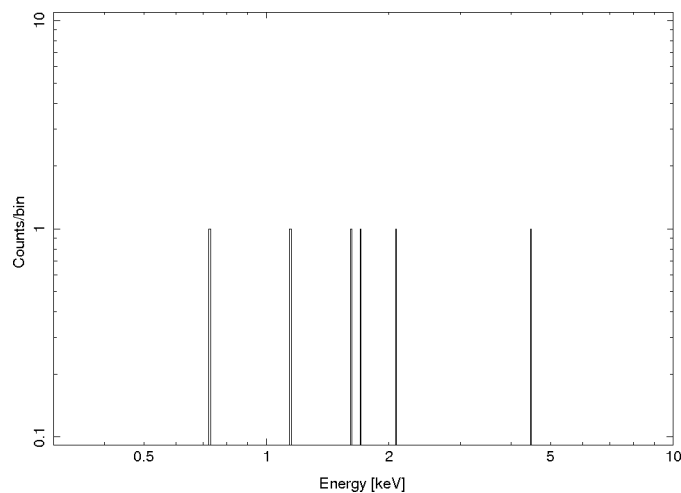


Figure 3.1: Spectrum of PKS 0055 – 328 plotted with ISIS

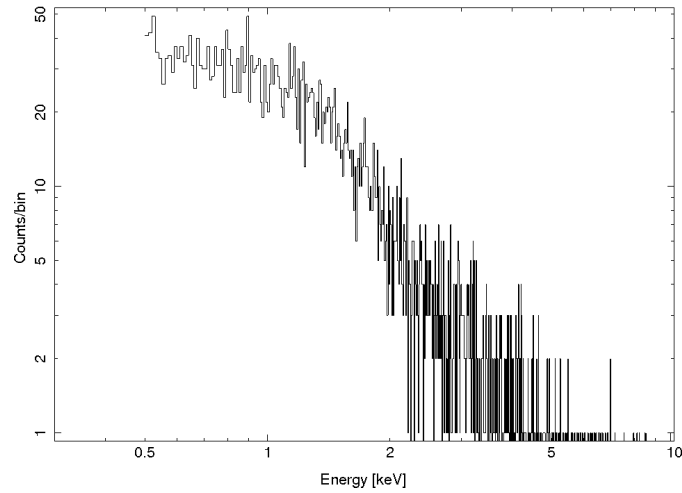


Figure 3.2: Spectrum of PKS 0447 – 439 plotted with ISIS

The jumps in the spectrum are due to single photons. The following spectra were grouped at a signal-to-noise ratio of 6.0. The spectrum of PKS 0447 – 439 (Fig. 3.2) rebinned is shown in Figure 3.3.

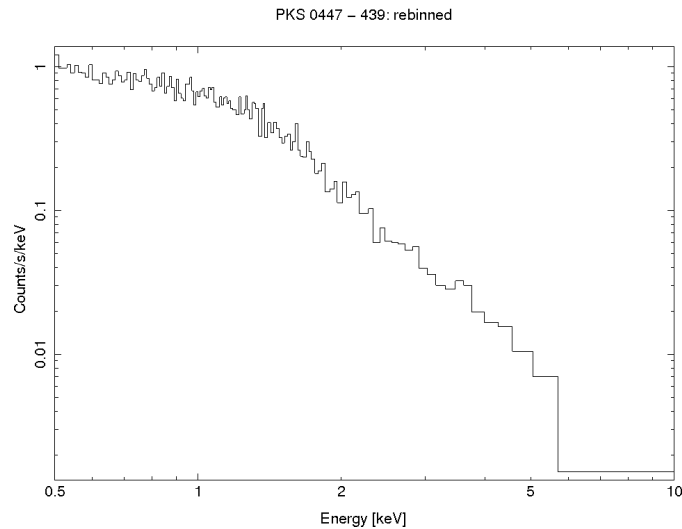


Figure 3.3: Spectrum of PKS 0447 – 439 rebinned

In this case data above 5 keV have been ignored and not used for fitting as the signal to noise ratio is too low. This is how most fits were done. In a few cases the energy range that was used for the fit extended to 4 keV or 6 keV. After grouping the data was fitted with the model described above.

Following are the results of the fitted spectra. All source information is from the NED database(<http://nedwww.ipac.caltech.edu/>), unless noted otherwise.

## 3.2 Bright sources

**PKS 0208 – 512** PKS 0208 – 512 is a radio-loud BL Lac type source, that was only barely visible in X-ray. This source has also been detected at MeV energies (Blom et al., 1995).

1.)

Table 3.1: Overview

Name	PKS 0208 – 512
Type	BL Lac
Coordinates	32.6925, -51.01722
z	1.003
d	4.0 Gpc

2.) Fit

Since this source was not visible very well in X-ray several Spectra were added. The timespan between the observations was roughly a month. The total (added) exposure time was 29.67 ks.

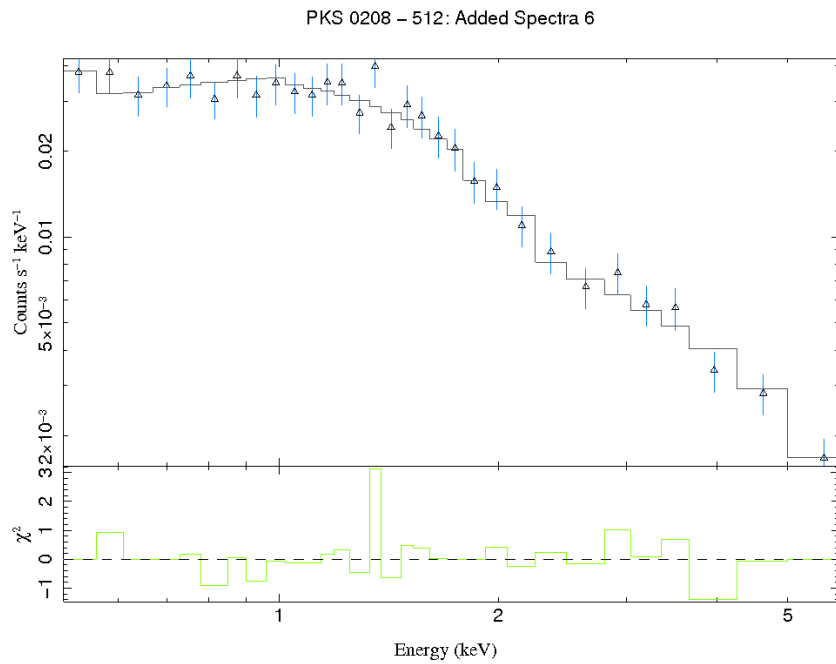


Figure 3.4: ObsID: 00035002001, 00035002002, 00035002003, 00035002004, 00035002005

## 3.) Parameters

The parameters fitted for several added spectra can be viewed in Table 3.2. DOF is the abbreviation for degrees of freedom and shows the number of bins after rebinning the spectrum.

Table 3.2: Fit Parameters

ObsID	Phabs.NH	C	$\Gamma$	red. $\chi^2$	DOF	t
Units	$\cdot 10^{22} \text{ cm}^{-2}$					ks
Added Spectra 2	$0.07^{+0.09}_{-0.07}$	$(3.2^{+1.1}_{-0.8}) \times 10^{-4}$	$1.9 \pm 0.4$	0.8223	11	16.13
Added Spectra 3	$0.09 \pm 0.06$	$(3.9^{+0.9}_{-0.7}) \times 10^{-4}$	$1.9 \pm 0.2$	0.7092	19	30.26
Added Spectra 4	$0.04^{+0.05}_{-0.04}$	$(4.4^{+0.9}_{-0.7}) \times 10^{-4}$	$1.65^{+0.19}_{-0.17}$	0.9960	23	19.05
Added Spectra 6	$0.03^{+0.05}_{-0.03}$	$(0.52^{+0.09}_{-0.07}) \times 10^{-3}$	$1.75^{+0.16}_{-0.14}$	0.4586	31	20.62
average	$0.06 \pm 0.12$	$4.2 \pm 1.7 \cdot 10^{-4}$	$1.79 \pm 0.5$	0.7465		

**PMNJ 0334 – 3725** Not much is known about PMNJ 0334 – 3725. The source was observed during the 2MASS (2 Micron All Sky Survey). No papers are available on this source.

## 1.)

Table 3.3: Overview

Name	PMNJ 0334 – 3725
Type	?
Coordinates	53.56425, -37.428806
z	?
d	?

## 2.) Fit

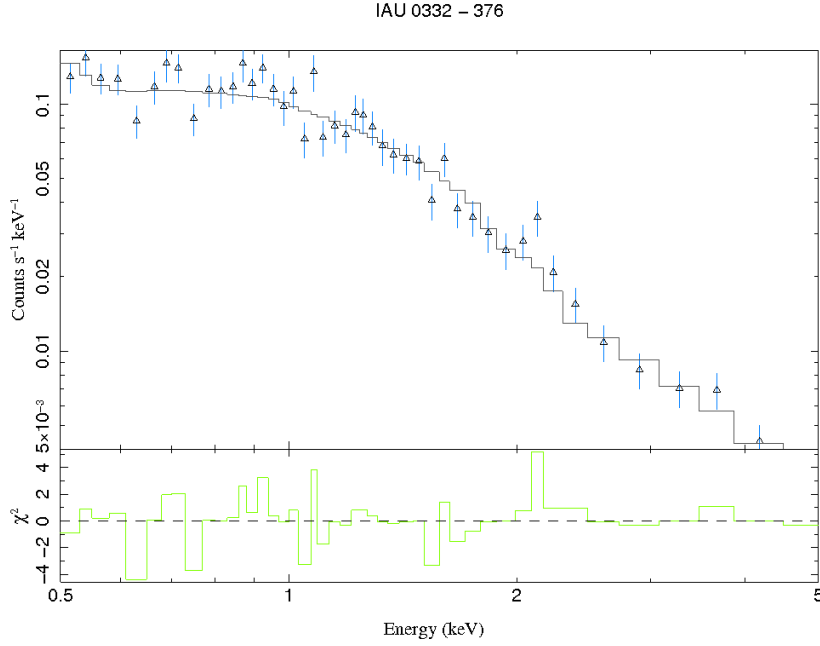


Figure 3.5: ObsID: 00038486002

## 3.) Fit Parameters

Table 3.4 shows the Fit Parameters with  $t$  being the exposure time in kiloseconds of each observation and n.d. the abbreviation for not determinable. In this case the parameter errors were too high. The time is the added exposure time in kiloseconds. It is a radio-loud source

Table 3.4: Fit Parameters

ObsID	$N_{\text{H}} \cdot 10^{22} \text{ cm}^{-2}$	$C \cdot 10^{-3}$	$\Gamma$	red. $\chi^2$	red. $\chi^2 N_{\text{H}}$	DOF	$t$
00038486001	$0.03^{+0.06}_{-0.03}$	$(0.63^{+0.16}_{-0.10})$	$2.5^{+0.3}_{-0.2}$	1.1143	1.0534	18	11.20
00038486002	$0.05^{+0.04}_{-0.03}$	$(1.5 \pm 0.2)$	$2.42^{+0.15}_{-0.14}$	1.1889	1.2265	46	13.61
00037557003	$0.03^{+0.05}_{-0.03}$	$(1.0 \pm 0.2)$	$2.1 \pm 0.2$	1.0650	1.0396	28	10.51
00037557004	n.d.	n.d.	$2.09^{+0.17}_{-0.10}$	0.9968	0.9943	26	8.73
00037557005	n.d.	$(1.15^{+0.10}_{-0.06})$	$2.09^{+0.10}_{-0.08}$	1.1172	1.1365	39	12.07
average	$0.0378 \pm 0.0696$	$1.0 \pm 0.86$	$2.2312 \pm 0.39$	1.0964	1.0901		

and has not been classified yet.

**QSO J0403-3605** QSO J0403 – 3605 is a low polarization quasar at a high redshift (Tornainen et al., 2005).

1.)

Table 3.5: Overview

Name	QSO J0403 – 3605
Type	Quasar
Coordinates	60.9739579, -36.0838644
z	1.42
d	5.66 Gpc

2.) Fit

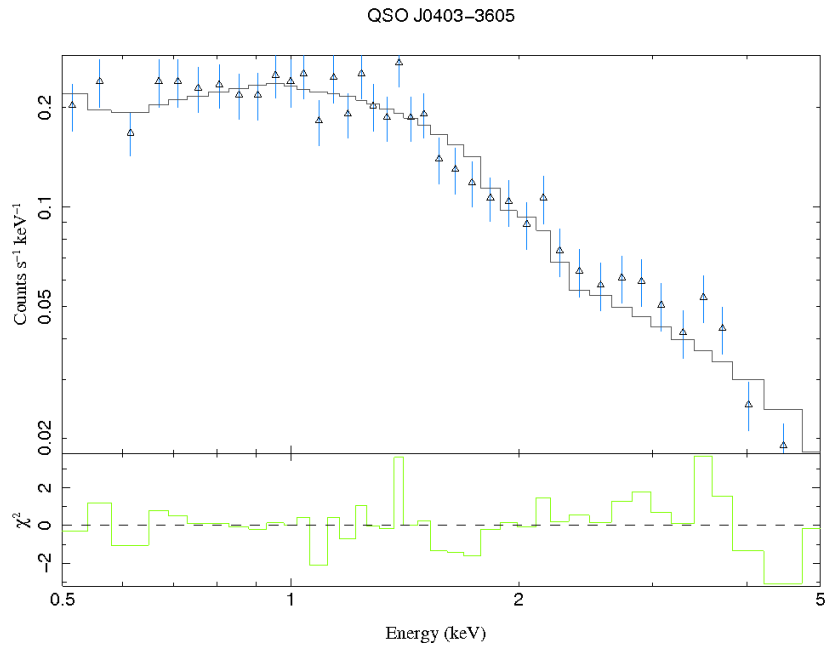


Figure 3.6: ObsID: 00036504006

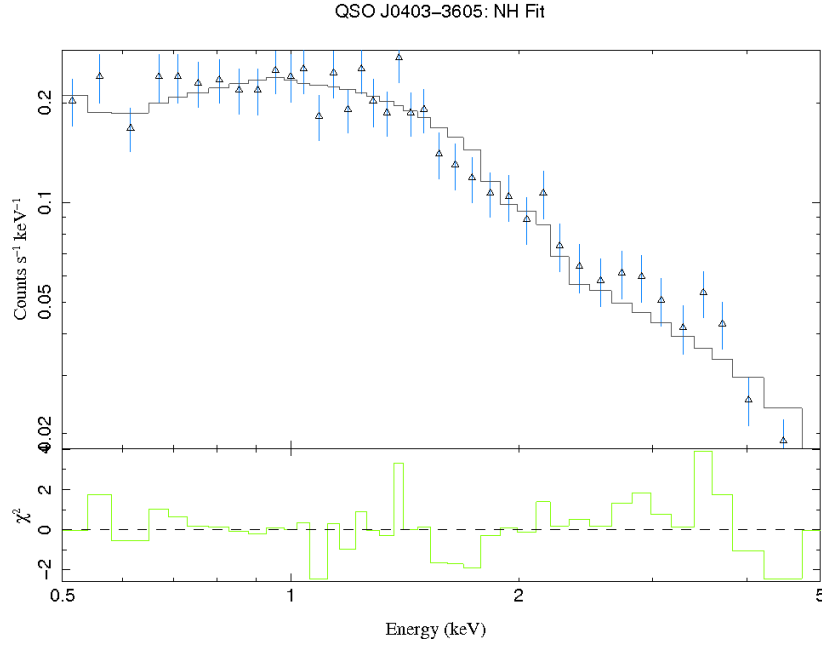


Figure 3.7: ObsID: 00036504006

## 3.) Fit Parameters

As a few observations couldn't be fitted as they only had few bins left after grouping the data, an added spectrum was made. The timespan is a day.

Table 3.6: Fit Parameters

ObsID	$N_{\text{H}} \cdot 10^{22} \text{ cm}^{-2}$	$C \cdot 10^{-3}$	$\Gamma$	red. $\chi^2$	red. $\chi^2(N_{\text{H}})$	DOF	t
00036504004	$0.07^{+0.04}_{-0.06}$	$(0.62^{+0.08}_{-0.12})$	$1.9^{+0.1}_{-0.2}$	0.8778	0.8380	24	14.21
00036504005	$0.01^{+0.07}_{-0.01}$	n.d.	$1.6^{+0.3}_{-0.2}$	0.7102	0.7726	14	1.03
00036504006	$0.04 \pm 0.04$	$(3.2^{+0.5}_{-0.4})$	$1.66 \pm 0.14$	0.9034	0.8940	40	3.78
added Spectrum	$0.06 \pm 0.04$	$(3.3^{+0.5}_{-0.4})$	$1.70 \pm 0.14$	1.1227		56	4.77
average	$0.0423 \pm 0.085$	$2.7 \pm 0.644$	$1.717 \pm 0.35$	0.9036	0.8349		

**PKS 0447 – 439** PKS 0447 – 439 was one of the brightest sources in my sample of observations. In 2009, H.E.S.S. observed VHE ( $E > 100$ ) GeV emission from the source, however, not much has been published about this source (Raue et al., 2009).

1.)

Table 3.7: Overview

Name	PKS 0447 – 439
Type	BL Lac
Coordinates	72.35292, -43.83583
z	0.107
d	445.5 Mpc

2.) Fit

In most cases there were 2 or more observations that have been fitted. Here I will show a typical plot of the sample of observations.

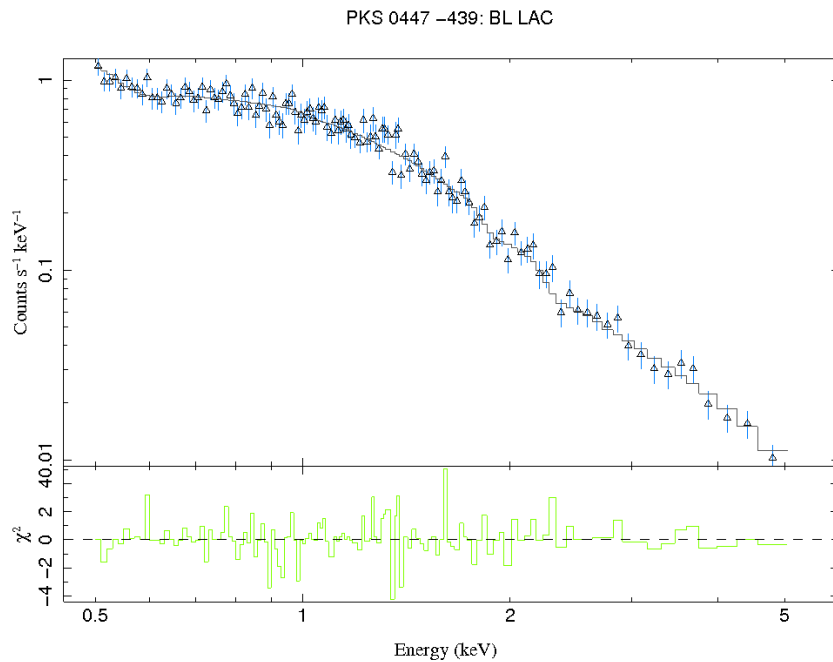


Figure 3.8: ObsID: 000383750001

3.) Fit and  $N_{\text{H}}$  Fit

The observation 00038375001 shows an interesting feature in the  $N_{\text{H}}$  Fit.

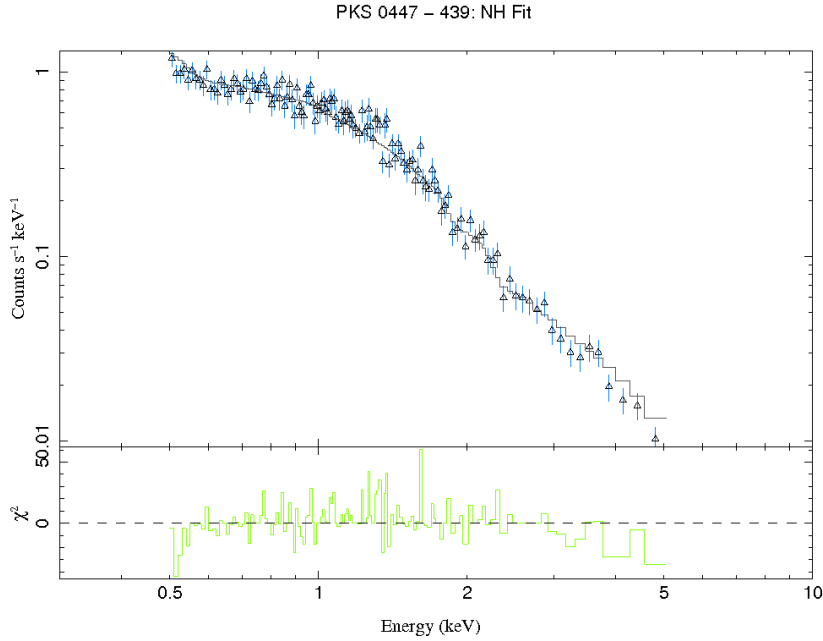


Figure 3.9: ObsID: 000383750001

This Fit shows a downward trend on the right as well as on the left side. Also the  $\chi^2$  Parameter in the  $N_{\text{H}}$  Fit is significantly worse than in the fit with free parameters. ( $\chi^2 = 100.3$  and  $\chi^2_{N_{\text{H}}} = 122.5$ ) This can be interpreted as a higher absorption, as the fitted photon absorption is  $6.6 \cdot 10^{20} \text{ cm}^{-2}$  whereas the galactic absorption has been measure to  $1.2 \cdot 10^{20} \text{ cm}^{-2}$ .

## 4.) Parameters

Table 3.8: Fit Parameters

ObsID	$N_{\text{H}} \cdot 10^{22} \text{ cm}^{-2}$	$C \cdot 10^{-3}$	$\Gamma$	red. $\chi^2$	red. $\chi^2(N_{\text{H}})$	DOF	t
00038100001	$0.07^{+0.03}_{-0.02}$	$12.5^{+1.2}_{-1.0}$	$2.54^{+0.11}_{-0.10}$	1.003957	1.185826	85	3.52
00038100002	$0.08^{+0.07}_{-0.06}$	$5.5^{+1.5}_{-1.1}$	$2.85 \pm 0.3$	0.7587857	0.9381929	18	1.55
00038100003	$0.124^{+0.014}_{-0.012}$	$9.0^{+0.6}_{-0.5}$	$2.97^{+0.12}_{-0.11}$	0.8267651	0.9741483	43	2.84
00038100005	$0.08 \pm 0.05$	$13.0^{+3.0}_{-2.0}$	$2.6 \pm 0.2$	0.8870307	1.090172	29	1.00
00038100006	$0.06 \pm 0.03$	$10.5^{+1.2}_{-1.1}$	$2.49^{+0.14}_{-0.13}$	0.8933746	0.9982979	63	2.83
00038100007	$0.10^{+0.06}_{-0.05}$	$7.9^{+1.7}_{-1.4}$	$2.6^{+0.3}_{-0.2}$	1.482727	1.76845	26	1.54
00038100008	$0.07^{+0.04}_{-0.03}$	$7.0^{+1.0}_{-0.8}$	$2.59^{+0.16}_{-0.15}$	1.055683	1.176418	49	3.13
00038100009	$0.10^{+0.03}_{-0.09}$	$7.0^{+0.0}_{-2.0}$	$2.9^{+0.1}_{-0.5}$	0.7010282	0.7944586	19	1.29
00038100010	$0.08 \pm 0.03$	$(6.6^{+0.8}_{-0.7})$	$2.82^{+0.15}_{-0.14}$	1.195931	1.39917	58	4.80
00038375001	$0.066^{+0.020}_{-0.019}$	$10.0 \pm 0.7$	$2.77 \pm 0.09$	0.7897621	0.9569574	130	12.67
00038375002	$0.09^{+0.03}_{-0.02}$	$5.2^{+0.5}_{-0.4}$	$3.19^{+0.13}_{-0.12}$	0.8046085	1.100942	93	10.96
Average	$0.07 \pm 0.13$	$8.4 \pm 9.9$	$2.71 \pm 0.63$	0.9454	1.1257		

4.) Contour Plot:  $N_{\text{H}}$  - Photonindex

The following plot shows confidence levels for the Fit Parameters of the photon absorption as well as the photon index. The red, green and blue contours show 68%, 90% and 99% confidence, respectively.

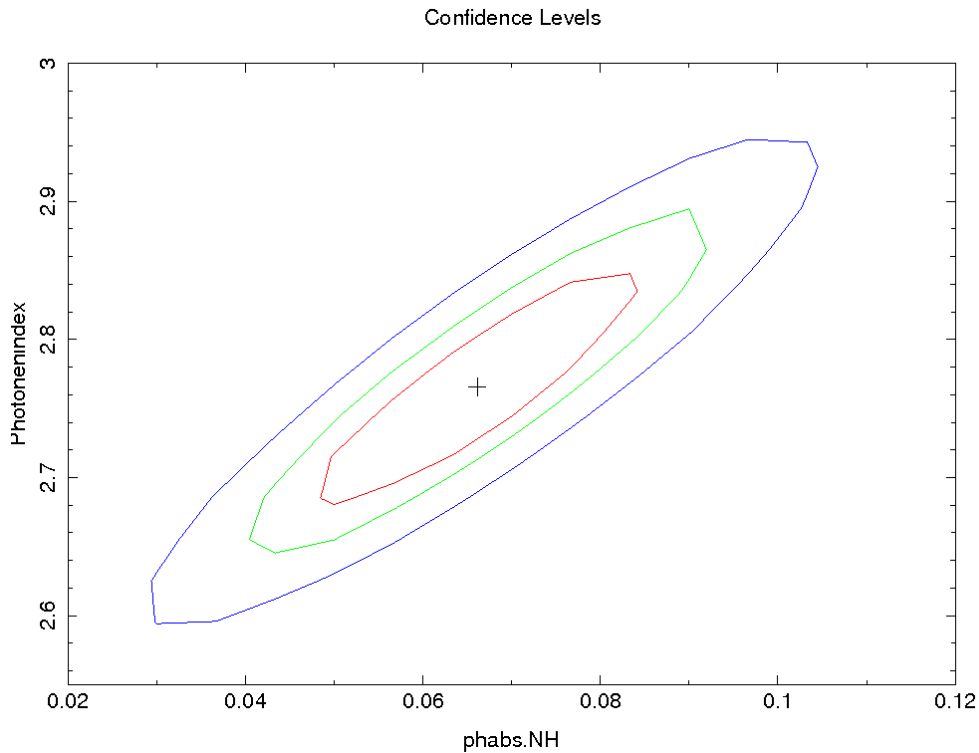


Figure 3.10: ObsID: 000383750001

The contour plot shows a correlation between the absorption and the steepness of the fitted powerlaw. This shows that the fit cannot distinguish between a high photon index with high absorption and a low photon index with less absorption. This correlation, however, is only of mathematical origin not physical.

**PKS 0506 – 61** PKS 0506 – 61 is a flat-spectrum quasar. Not much has been published about this source.

1.)

Table 3.9: Overview

Name	PKS 0506 – 61
Type	Quasar
Coordinates	76.68333, -61.16139
z	1.093
d	4.4 Gpc

2.) Fit

For this source only one observation was available.

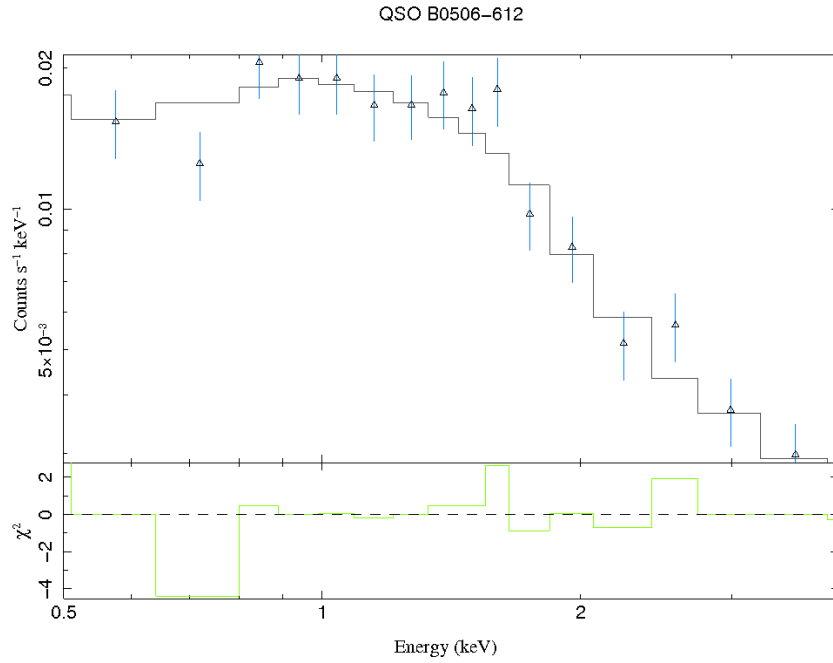


Figure 3.11: ObsID: 00038379001

3.) Parameters

Table 3.10: Fit Parameters

ObsID	$N_{\text{H}} \cdot 10^{22} \text{ cm}^{-2}$	$C \cdot 10^{-4}$	$\Gamma$	red. $\chi^2$	red. $\chi^2(N_{\text{H}})$	DOF	t
00038379001	$0.05^{+0.07}_{-0.05}$	$2.9^{+0.7}_{-0.6}$	$1.7 \pm 0.2$	1.0519	1.0314	18	20.16

**QSO B0521-365** Not much has been published about this source.

1.)

Table 3.11: Overview

Name	PKS 0521 – 036
Type	BL Lac
Coordinates	80.74167, -36.45861
z	0.055
d	221.2 Mpc

2.) Fit

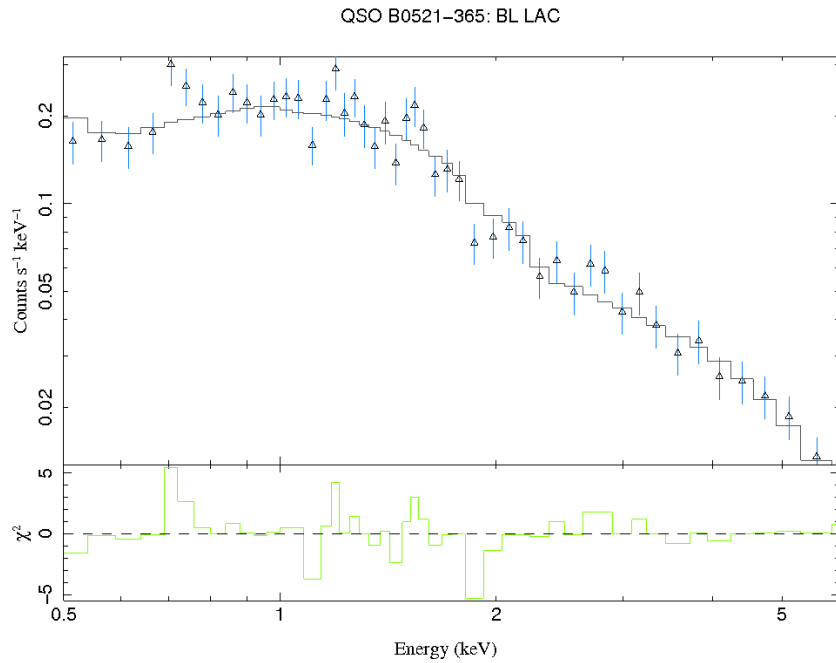


Figure 3.12: ObsID: 0005664004

3.) Parameter

Table 3.12: Fit Parameters

ObsID	$N_{\text{H}} \cdot 10^{22} \text{ cm}^{-2}$	$C \cdot 10^{-3}$	$\Gamma$	red. $\chi^2$	red. $\chi^2(N_{\text{H}})$	DOF	t
00056640004	$0.04^{+0.04}_{-0.03}$	$3.0^{+0.4}_{-0.3}$	$1.60 \pm 0.12$	1.0067	0.9855	49	4.92
00056640006	$0.09^{+0.05}_{-0.04}$	$2.8^{+0.5}_{-0.4}$	$1.72^{+0.16}_{-0.15}$	1.4242	1.4877	36	4.17
00056640007	$0.04^{+0.05}_{-0.04}$	$2.2 \pm 0.4$	$1.57^{+0.20}_{-0.18}$	0.9618	0.9181	24	2.94
Added spectra	$0.06 \pm 0.02$	$2.8 \pm 0.2$	$1.66 \pm 0.07$	1.0436		105	12.17
Average	$0.056 \pm 0.075$	$2.70 \pm 0.72$	$1.63 \pm 0.28$	1.1091	1.1305		

**PKS 0537 – 441** PKS 0537 – 441 is a highly polarized intra-day variable quasar. Romero et al. (Romero et al., 1995) suggest the presence of a foreground galaxy that causes superluminal microlensing.

1.)

Table 3.13: Overview

Name	PKS 0537 – 441
Type	Quasar
Coordinates	84.70958, -44.08583
z	0.896
d	3.6 Gpc

2.) Fit

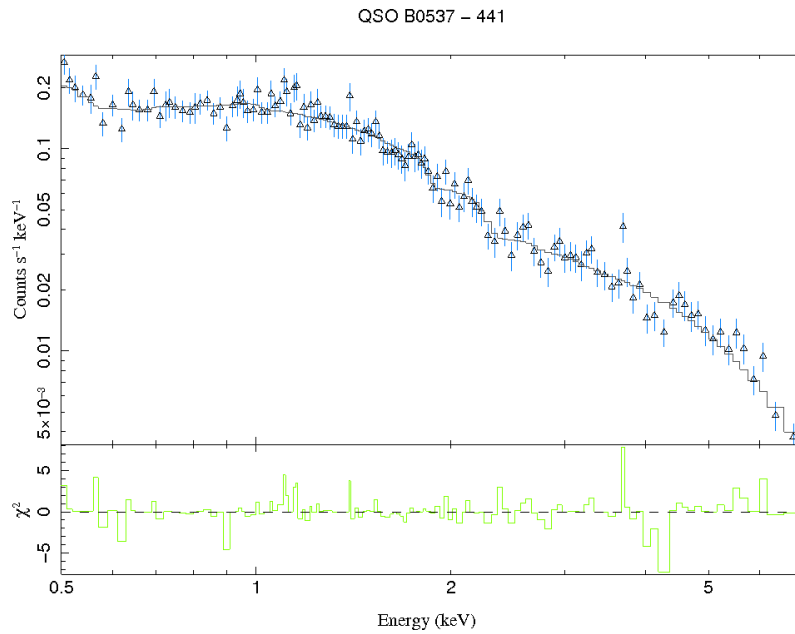


Figure 3.13: ObsID:00050150011

3.) Parameter

Table 3.14: Fit Parameters

ObsID	$N_{\text{H}} \cdot 10^{22} \text{ cm}^{-2}$	$C \cdot 10^{-3}$	$\Gamma$	red. $\chi^2$	red. $\chi^2(N_{\text{H}})$	DOF	t
00050150010	n.d.	n.d.	$1.6_{-0.1}^{+0.2}$	0.2608	0.3767	12	7.44
00050150011	n.d.	n.d.	$1.64_{-0.03}^{+0.05}$	0.869	0.9353	137	22.94
00050150012	$0.05 \pm 0.02$	$2.02_{-0.15}^{+0.16}$	$1.75_{-0.07}^{+0.08}$	0.8852	0.8892	106	18.59
added 1	$0.04 \pm 0.04$	$0.76_{-0.10}^{+0.11}$	$1.76 \pm 0.14$	0.7552		35	17.49
added 2	$0.09 \pm 0.05$	$1.1 \pm 0.2$	$1.81_{-0.18}^{+0.19}$	1.0554		27	11.60
added 3	$0.03_{-0.03}^{+0.05}$	$0.60_{-0.09}^{+0.12}$	$1.71_{-0.17}^{+0.19}$	0.5545		24	14.21
average	$0.04 \pm 0.078$	$1.2 \pm 0.29$	$1.72 \pm 0.34$	0.4028	0.7513		

**PKS 0625 – 35** The classification of the source is the origin of discussion, as is shown in section 3.4.1.

1.)

Table 3.15: Overview

Name	PKS 0625 – 35
Type	BL Lac?
Coordinates	96.77792, -35.4875
z	0.055
d	218.2 Mpc

2.) Fit

For this source only one observation was available.

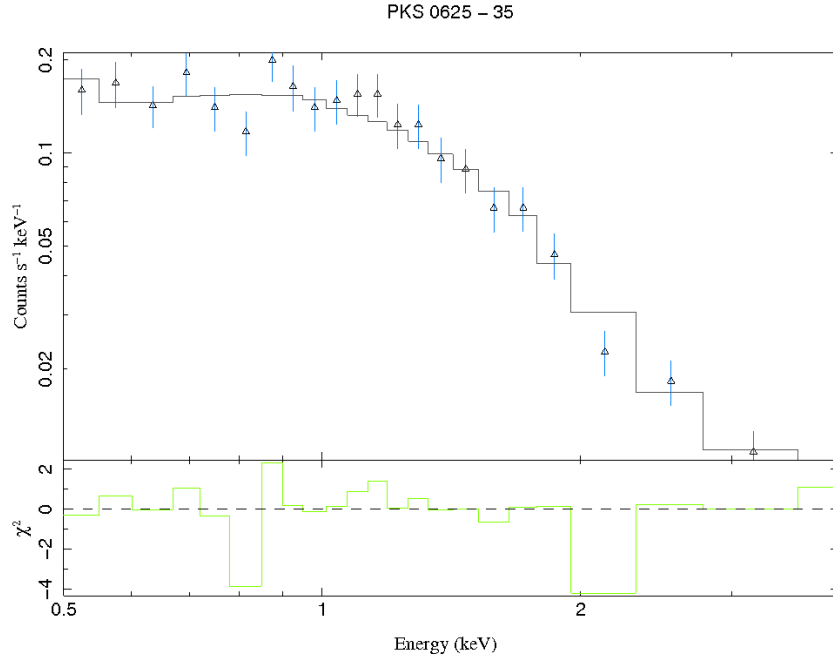


Figure 3.14: ObsID: 00039136002

3.) Parameter

Table 3.16: Fit Parameters

ObsID	$N_{\text{H}} \cdot 10^{22} \text{ cm}^{-2}$	$C \cdot 10^{-3}$	$\Gamma$	red. $\chi^2$	red. $\chi^2(N_{\text{H}})$	DOF	t
00039136002	$0.10 \pm 0.06$	$2.5^{+0.6}_{-0.5}$	$2.5 \pm 0.3$	0.9048	0.9045	23	4.55

**QSO B0637 – 752** Schwartz et al. observed a 100 kpc Jet of QSO B0637 – 752 in X-ray with Chandra (Schwartz et al., 2000). This jet could not be seen in the Swift observations, probably due to short exposures.

1.)

Table 3.17: Overview

Name	QSO B0637 – 752
Type	Quasar
Coordinates	98.94375, -75.27139
z	0.651
d	2.6 Gpc

2.) Fit

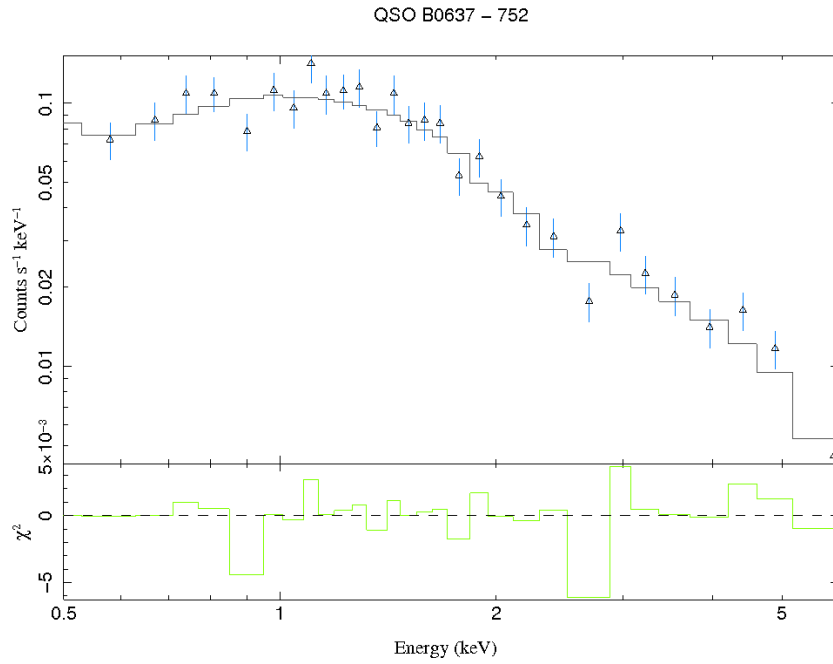


Figure 3.15: ObsID: 00037895006

3.) Parameter

Table 3.18: Fit Parameters

ObsID	$N_{\text{H}} \cdot 10^{22} \text{ cm}^{-2}$	$C \cdot 10^{-3}$	$\Gamma$	red. $\chi^2$	red. $\chi^2(N_{\text{H}})$	DOF	t
00037895005	$0.07^{+0.08}_{-0.06}$	$(1.3^{+0.4}_{-0.3}) \times 10^{-3}$	$1.7 \pm 0.3$	1.1450	1.0208	11	2.68
00037895006	$0.09^{+0.05}_{-0.04}$	$(1.7^{+0.3}_{-0.2}) \times 10^{-3}$	$1.70^{+0.16}_{-0.15}$	1.1829	1.1435	30	5.52
Average	$0.08 \pm 0.119$	$1.5 \pm 0.43 \cdot 10^{-3}$	$1.7 \pm 0.34$	1.1640	1.1229		

### 3.3 Weak sources

In the sample of TANAMI sources was a certain number of observations, that could not be modeled, as there were not enough counts:

Table 3.19: Sources and Exposure

Source	Exposure [ks]
PKS 0055-328	6.17
PKS 0227-369	12.3
PKS 0244-470	5.36
PKS 0302-623	12.17
PKS 0308-611	7.65
PKS 0332-403	8.68
PKS 0405-385	21.95
PMN J0413-5332	5.09
PMN J0428-3756	4.72
0454-463	5.87
PKS 0516-621	18.27
PKS 0524-485	12.89
PKS 0700-661	4.86

The given exposure time includes the total time of all observations for this source. Those observations with  $< 7$  ks of exposure time are probably underexposed and need a longer observation time. Sources with a long exposure have either too short exposure in each observation (and the spectra could not be added, due to the time between these observations) or they have to be looked at closer. Observations with long exposures and a low count rate is the case for PKS 0227-369, which was only one observation, PKS 0302-623 with only two observations, PKS 0405-385 with only three observations and a weak added spectrum, that could not be modeled, PKS 0516-621 with only one observation and PKS 0524-485 with two observations.

## 3.4 Analysis

### 3.4.1 Photon indices

Following is a short summary of the photon indices of the sources mentioned in the last section. Figure 3.16 shows the frequency of photon indices. It is obvious that the photon index of most

Table 3.20: Photon indices

Source	$\Gamma$	Type
PKS 0521-365	1.63	BL Lac
PKS 0332-403	1.64	Quasar
PKS 0506-61	1.68	Quasar
QSO B0637-752	1.705	Quasar
QSO J0403-3605	1.71	Quasar
PKS 0537-441	1.72	BL Lac
PKS 0208-512	1.8	BL Lac
PMN J0334-3725	2.27	?
PKS 0625-35	2.5	BL Lac?
PKS 0447-439	2.71	BL Lac

sources is between 1.6 and 1.8, although there is also an accumulation around 2.5. There is no classification of PMN J0334-3725 so far. There has been discussions about the classification about PKS 0625-35. VLA observations show radio lobes which would indicate a Radio Galaxy (Ekers et al., 1989).

Wills et al. (Wills et al., 2004), however, suggest that this AGN is a BL Lac type object. The photon index, that has been fitted, also suggests a BL Lac object.

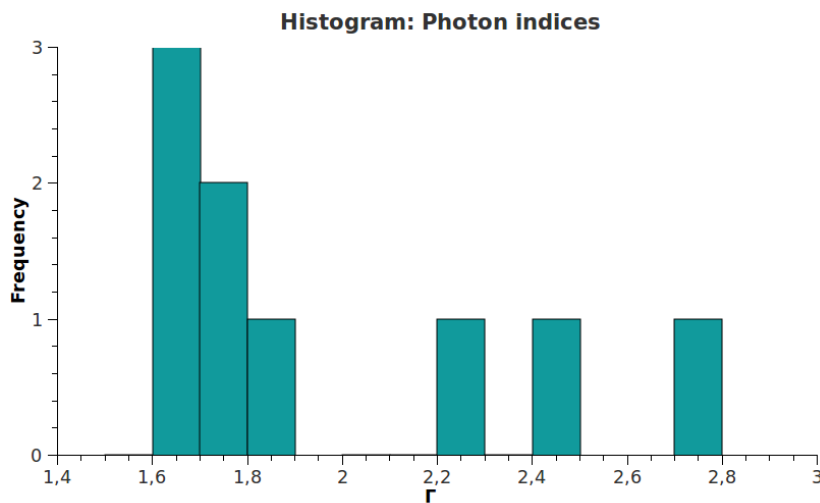


Figure 3.16: Histogram of Photon Indices

Now, considering the typical AGN broad-band spectra, one can take a closer look at the photon indices.

$$N_{ph} \propto E^{-\Gamma}$$

$$\begin{aligned}
 F_\nu &\propto E^{1-\Gamma} \\
 \nu F_\nu &\propto E^{2-\Gamma}
 \end{aligned}
 \tag{3.1}$$

From equation 3.1 follows that a Photon index  $\Gamma > 2$  is describing a falling slope, the slope of the Synchrotron peak, whereas a Photon index  $\Gamma < 2$  a rising slope of the Self-Compton hump. (See also Chapter 1) In the first case those blazars are called HBL: High frequency peaked blazars and the latter are called LBL: Low frequency peaked blazar. The gap in Figure 3.16 is due to the fact that a source is either a HBL or a LBL and cannot have a flat spectrum in a  $\nu F_\nu$  plot which would be equal to a photon index of 2. This is not observed since the flux in the valley would be very low and is unlikely to be detected. Figure 3.16 shows that most sources observed are LBLs, which makes sense, as LBLs are generally more luminous than HBLs.

### 3.4.2 Absorption

In all observations the fitted absorption is not much higher than that of the measured galactic NH. The parameter was within  $1 - 10 \cdot 10^{20} \frac{1}{\text{cm}^2}$ . For a higher absorption one would expect an absorption of  $\approx 10^{22} \frac{1}{\text{cm}^2}$

## Chapter 4

# Summary and Outlook

Conclusively I can say that the assumption if a power law fits very well with the results. In the future more multiwavelength campaigns with long exposure are necessary to understand active galaxies better. Hopefully, future projects like the eROSITA will deliver better observations which will lead to a deeper understanding of the underlying physical processes.

# Chapter 5

## Appendix

### 5.0.3 Added Spectra

**PKS 0208 – 512** For this source Spectra 2 was an added spectrum of following observations: 00035002033, 00035002034, 00035002035, 00035002036, 00035002037, 00035002038, 00035002039, 00035002040, 00035002041, 00035002042, 00035002043, 00035002044. These observations were made over a timespan of 3 months.

Spectra 3 consists of the following observations: 00035002022, 00035002023, 00035002024, 00035002025, 00035002026, 00035002027, 00035002028, 00035002029, 00035002030, 00035002031. The timespan was 1 month.

Spectra 4 consists of the following observations: 00035002008, 00035002009, 00035002010, 00035002012, 00035002013, 00035002014, 00035002015, 00035002016, 00035002017, 00035002018, 00035002020, 00035002021. The timespan was 2 months.

Spectra 6 consists of the following observations: 00038462001, 00035002001, 00035002002, 00035002003, 00035002004, 00035002005. The timespan was 1 month.

**QSO J0403-3605** For this source one added spectrum was made. It consisted of following observations: 00036504005, 00036504006. The timespan was 1 day.

**QSO B0521-365** For this source one added spectrum was made. It consisted of following observations: 00056640004, 00056640005, 00056640006, 00056640007 . The timespan was 2 weeks.

**PKS 0537 – 441** For this source several added spectra were made, due to the large number of observations. Spectra 1 consists of 00030138001, 00030138002, 00030138003. The timespan was 4 months.

Spectra 2 consists of 00030138004, 00030138005, 00030138006, 00030138007, 00030138008, 00030138009. The timespan was 2 weeks.

Spectra 3 consists of 00030138019, 00030138020, 00030138021, 00030138022. The timespan was 2 months.

# Bibliography

- Baade W., Minkowski R., 1954, *ApJ* 119, 206
- Blom J.J., Bennett K., Bloemen H., et al., 1995, *A&A* 298, L33+
- Boeck M., Kadler M., Tosti G., et al., 2010, ArXiv e-prints
- Burrows D.N., Hill J.E., Nousek J.A., et al., 2005, *Space Sci. Rev.* 120, 165
- Curtis H.D., 1918, *Publications of Lick Observatory* 13, 9
- Ekers R.D., Wall J.V., Shaver P.A., et al., 1989, *MNRAS* 236, 737
- Fath E.A., 1909, *Lick Observatory Bulletin* 5, 71
- Ghisellini G., 2009, *Mem. Soc. Astron. Ital.* 80, 201
- Godet O., Beardmore A.P., Abbey A.F., et al., 2009, *A&A* 494, 775
- Godet O., Beardmore A.P., Abbey A.F., et al., 2007, In: *Society of Photo-Optical Instrumentation Engineers (SPIE) Conference Series*, Vol. 6686. Society of Photo-Optical Instrumentation Engineers (SPIE) Conference Series
- Holland S.T., 2010, *The Swift Technical Handbook*, [http://swift.gsfc.nasa.gov/docs/swift/proposals/tech\\_appd/ta/ta.html](http://swift.gsfc.nasa.gov/docs/swift/proposals/tech_appd/ta/ta.html)
- Kadler M., 2010, <http://pulsar.sternwarte.uni-erlangen.de/tanami/>
- Kalberla P.M.W., Burton W.B., Hartmann D., et al., 2005, *A&A* 440, 775
- Kemhavi A.K., Narlika Jayant V., 1999, *Quasars and Active Galactic Nuclei*, Cambridge University Press, Cambridge, United Kingdom
- Krolik J.H., 1999, *Active Galactic Nuclei*, Princeton University Press, Princeton, New Jersey, USA
- Müller C., Kadler M., Ojha R., et al., 2010, In: A. Comastri, L. Angelini, & M. Cappi (ed.) *American Institute of Physics Conference Series*, Vol. 1248. American Institute of Physics Conference Series, p.481
- Ojha R., Kadler M., Böck M., et al., 2010a, ArXiv e-prints
- Ojha R., Kadler M., Boeck M., et al., 2010b, ArXiv e-prints
- Peterson B.M., 2009, *An Introduction to Active Galactic Nuclei*, Cambridge University Press, Cambridge, United Kingdom
- Raue M., Behera B., Charbonnier A., et al., 2009, *The Astronomer's Telegram* 2350, 1

- Romero G.E., Surpi G., Vucetich H., 1995, *A&A* 301, 641
- Sanderson A., 2007, <http://www.sr.bham.ac.uk/~ajrs/R/r-gallery.html>
- Schwartz D.A., Marshall H.L., Lovell J.E.J., et al., 2000, *ApJ* 540, L69+
- Seyfert C.K., 1943, *ApJ* 97, 28
- Suchy S., Pottschmidt K., Wilms J., et al., 2008, *ApJ* 675, 1487
- Torniainen I., Tornikoski M., Teräsranata H., et al., 2005, *A&A* 435, 839
- Trussoni E., Vagnetti F., Massaglia S., et al., 1999, In: B. Aschenbach & M. J. Freyberg (ed.) *Highlights in X-ray Astronomy.*, p.185
- Urry C.M., Padovani P., 1995, *PASP* 107, 803
- Wills K.A., Morganti R., Tadhunter C.N., et al., 2004, *MNRAS* 347, 771
- Wilms J., Kadler M., 2010, *Active Galactic Nuclei, Lecture ST 2010 University Erlangen-Nürnberg*

# Acknowledgement

I would like to thank everybody for the support during the time of this bachelor thesis. In particular I give many thanks to

- M. Kadler and J. Wilms for much help and support.
- all the „Remeisen“ at the Dr. Remeis observatory in Bamberg, especially to Laura Baragán for the help with the xrt scripts, as well as Manfred Hanke, Moritz Böck, Cornelia Müller and Felix Fürst.
- J. Veh, M. Müller, T. Beuchert and B. Falkner for the helpful discussions and the moral support.
- C. Stegmann for the helpful discussion

# Erklärung

Hiermit bestätige ich, dass ich diese Arbeit selbstständig und nur unter Verwendung der angegebenen Hilfsmittel angefertigt habe.

Erlangen, den 12.08.2010

---

Felicia Krauß